Available online at www.sciencedirect.com
SCIENCE DIRECT
Journal of Colloid and Interface Science 278 (2004) 393–403
JOURNAL OF Colloid and Interface Science
www.elsevier.com/locate/jcis

Inhibition of steel corrosion by calcium benzoate adsorption in nitrate solutions: theoretical and experimental approaches

G. Blustein [a], C.F. Zinola [b,*]

[a] *Centro de Investigación y Desarrollo en Tecnología de Pinturas, CIC-CONICET, Postal Code 1900, La Plata, Argentina*
[b] *Laboratorio de Electroquímica Fundamental, Facultad de Ciencias, Universidad de la República, Libertad No. 2497, Postal Code 11300, Montevideo, Uruguay*

Received 16 January 2004; accepted 2 June 2004

Available online 10 July 2004

Abstract

The inhibitive effects of calcium benzoate on steel corrosion were studied in sodium nitrate solutions at room temperature. Corrosion parameters of the steel/nitrate and steel/benzoate + nitrate interfaces were obtained from polarization curves. Adsorption parameters of benzoate on steel in sodium nitrate solutions were determined through changes in the degree of surface coverage by the inhibitor, as a function of concentration, time, and adsorption potential. The most likely adsorption configuration of benzoate on iron was envisaged with the help of semiempirical calculations such as extended Hückel calculations. A two-dimensional flat configuration was involving at least two metal atoms, one interacting with the phenolic group and the other with the carboxylate moiety. The effect of chloride on the corrosion inhibition of benzoate was analyzed by exposing the metal to different chloride solution concentrations, from which corrosion parameters were calculated and compared with those in nitrate solutions.
© 2004 Elsevier Inc. All rights reserved.

Keywords: Steel; Inhibition; EHMO calculations; Adsorption; Calcium benzoate

1. Introduction

Steel has found wide applications in a broad spectrum of industries and machinery; however its tendency to corrosion makes it inadequate for marine atmospheres. The industry of steel and iron starves for the incorporation of the proper methodology for metal protection in each application. The use of inhibitors is one of the most widespread strategies to restrain corrosion [1–3]. Two types of corrosion inhibitors are of special interest for protection: adsorption inhibitors in acid corrosion and metal passivation [4]. The inhibitors for acid corrosion have extensive engineering importance in the pickling of scaled metals and in the production of natural gas and oil. Investigations conducted on corrosion inhibition in acid media showed that a great number of effective inhibitors are organic species containing nitrogen, oxygen, and/or sulfur [4–6]. The inhibitive action arises from adsorption onto the metal surface of the functional groups contained in the organic compound. This results in a decrease of the anodic and/or cathodic reaction kinetics responsible for metal corrosion in aggressive environments [5–7]. Many mono- and polyfunctional organic inhibitors are being described in the current literature by their efficiencies to corrosion inhibition, as well as their adsorption characteristics [8–18]. A detailed list of dosages of these inhibitors to restrain metal corrosion can be found in the review by Fontana and Greene [19].

Different electrochemical techniques such as linear polarization curves, cyclic polarization tests, electrochemical impedance spectroscopy, and surface scanning with ultramicroelectrodes have been used to envisage the mechanism of corrosion inhibition on various metals [20–22]. From the pioneer work and of Bockris [23,24], the importance of including in situ spectroelectrochemical methodologies as complementary tools for the investigation of inhibitor adsorption has also been shown.

Benzoate compounds offer interesting possibilities for corrosion inhibition and are of particular interest because of their safe use and high solubility in water [25–34]. The influence of benzoate concentration, pH, and dissolved oxy-

* Corresponding author. Fax: +5982-525-07-49.
E-mail address: fzinola@fcien.edu.uy (C.F. Zinola).

0021-9797/$ – see front matter © 2004 Elsevier Inc. All rights reserved.
doi:10.1016/j.jcis.2004.06.009

gen on the corrosion of pure annealed iron was studied, employing sodium benzoate solutions [24,25,32]. The inhibition effect of benzoate was attributed to the blocking of surface sites in the anodic dissolution by the inhibitor molecule. According to the literature [27,32], the degree of adsorption by benzoate compounds on ferrous metals follows the Langmuir isotherm. Moreover, the adsorption of the inhibitor competes with that of anions such as chloride and sulfate [28].

The corrosion inhibition of carbon steel by blends of gluconate and benzoate and blends of benzoate and acetate was also reported as a new possibility for their use [29,30]. Sodium benzoate and *p*-substituted benzoic acid derivatives were employed as corrosion inhibitors for aluminum in acid media [31,33,34].

An increasing interest in the use of organic inhibitors in the field of paint technology has grown up during the past decade. Many of these inhibitors were found to improve the anticorrosive behavior of inorganic pigments [35–39]. Among these inhibitors, the salts formed by benzoic acid and bivalent cations, such as calcium and zinc, have gained acceptance due to the inhibitive properties of the anion [35–37], which may be enhanced by the presence of the cation [40,41]. Moreover, it has been found that metallic benzoates are also useful to reduce "flash rusting" in waterborne paints [42].

In this work, the adsorption parameters that characterize the inhibition effects of calcium benzoate on steel are approached by classical electrochemical techniques in sodium nitrate solutions. The adsorption configurations of neutral benzoate on pure iron single crystals were calculated using the extended Hückel molecular orbital (EHMO) methodology.

2. Experimental

2.1. Materials and solutions

A three-electrode compartment cell was used for electrochemical and adsorption measurements (cyclic voltammetry, electrochemical adsorption, and polarization curves). The working electrodes were made from SAE 1010 steel rods. They were embedded with a polyurethane coating to ensure that no changes in the surface area (0.122 cm^2) occurred during polarization. Before that, all the working electrodes were mechanically polished with emery paper up to a 1200 grid and subsequently rinsed in ultrapure water from APS Ultrawater.

The counterelectrode was a large-area platinum electrode (ca. 20 cm^2) and the reference electrode a saturated calomel device in a double-fritted glass compartment to minimize chloride diffusion. The supporting electrolyte was prepared with sodium nitrate (99.998%, Merck), the working solutions with the addition of calcium benzoate (labprepared with benzoic acid, ammonium hydroxide, and calcium nitrate) and/or sodium chloride (99.99%, Merck) with APS Ultrawater ($\rho > 18.2\ M\Omega\ cm$).

2.2. Equipment

The electrochemical experiments were performed using a PGP Radiometer potentiostat–galvanostat with Voltamaster 1 software.

Alternatively, the surface morphology of steel, previously subjected to distinct electrolyte solutions for 48 h, was analyzed by a Phillips SEM 505 scanning electron microscope coupled with an EDAX OX Prime 10 (energy-dispersed form).

The reflectance spectra were recorded with a GBC CINTRA 40/UV–visible spectrometer, which operated between 190 and 1000 nm. Spectra were scanned over the range 200–800 nm.

2.3. Technical methodologies

Before the adsorption and polarization experiments, cyclic voltammetry was run at 0.50 $V\,min^{-1}$ between the solvent stability potentials to obtain the electrochemical spectra of steel in the different electrolyte solutions.

2.3.1. Polarization curves

Linear sweep polarization curves were obtained by scanning the working electrode in the ±0.10-V range from the open-circuit potential of the steel/electrolyte interface at 0.05 $V\,min^{-1}$. Corrosion current densities (j_{corr}) and corrosion potentials (E_{corr}) were evaluated from the intersection of the linear anodic and cathodic branches of the polarization curves as Tafel plots. They were calculated by lineal regressions in the ±0.05-V linear ranges from the open circuit potential with the Voltamaster 1 software.

2.3.2. Adsorption isotherms

The adsorption isotherms were constructed by evaluating j_{corr} in the presence and in the absence of the inhibitor ($j_{corr,o}$). All measurements were carried out in normally oxygenated solutions without stirring and at room temperature (20 °C).

The surface coverage of the steel electrode by benzoate (θ) in nitrate solutions was determined at different calcium benzoate bulk concentrations (C), adsorption times (t_{ads}), and adsorption potentials (E_{ads}). In this method, it is assumed that the inhibitor is homogeneously distributed on the steel surface and only a monolayer is formed on the electrode [48–50]. Thus, on the basis of this consideration, the value of θ is

$$\theta = 1 - \frac{j_{corr}}{j_{corr,o}}. \quad (1)$$

According to the literature [27,32] the adsorption of aromatic-containing compounds on ferrous metals can obey Langmuir, Temkin, or Frumkin isotherms. They were

checked in the $10^{-5} < C < 10^{-1}$ M range at $t_{ads} = 20$ min and at the open circuit potential. Moreover, in the case of $C = 10^{-2}$ M, t_{ads} was varied from 0 to 60 min. On the other hand, θ values were also evaluated varying E_{ads} from the open-circuit potential ±0.30 V in $C = 10^{-2}$ M, all at $t_{ads} = 30$ min.

2.4. The influence of chloride in solution

The effect of chloride on the inhibition of steel corrosion caused by benzoate was studied following the routines described below:

Routine A. First, benzoate was adsorbed on steel in 0.10 M calcium benzoate + 0.70 M sodium for nitrate solution 30 min at the open-circuit potential. Second, the steel surface was put in a solution of 0.10 M benzoate + 0.70 M nitrate containing different concentrations of sodium chloride (0.01, 0.10, and 0.40 M) at the new open-circuit potential for 10 min. Finally, the polarization curve was run in those solutions at 0.05 V min^{-1} within the ±0.10-V domain from the open-circuit potential. From the linear lines the corrosion parameters were determined.

Routine B. First, the steel surface was put in contact with 0.10 M calcium benzoate + 0.70 M sodium nitrate solution for 30 min at the open-circuit potential. Second, the passivation of the surface was accomplished at 0.40 V for 10 min in the same solution, and third, the electrode was put into contact with a solution containing 0.40 M sodium chloride + 0.10 M calcium benzoate + 0.70 M sodium nitrate at the new open-circuit potential, also for 10 min. Finally, the polarization curve was run at 0.05 V min^{-1} in the ±0.10-V domain from the open-circuit potential to determine the corrosion parameters.

Routine B was repeated under similar conditions, but without calcium benzoate, and in another case without solution chloride, for comparison purposes.

3. Results and discussion

3.1. Electrochemical and surface characterization of SAE 1010 steel in the presence of calcium benzoate

The cyclic voltammogram of an SAE 1010 steel surface in oxygen-free 0.70 M sodium nitrate run at 0.50 V min^{-1} is shown in Fig. 1. The anodic profile exhibits a complex contour of four peaks with onset potential of steel oxidation ca. −0.7 V, which corresponds to the formation of a monolayer of ferrous oxide [43]. The first stage of steel oxidation defines an anodic peak at −0.60 V, whereas the formation of the two bulk iron oxides occurs at −0.40 and 0 V, respectively. The fourth peak appeared at ca. 0.25 V, like a hump of the third peak. The passivation of the steel surface in the electrolyte took place from

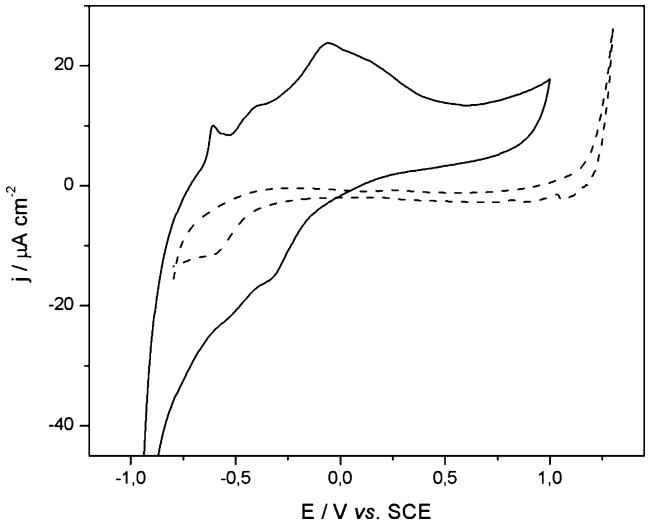

Fig. 1. Cyclic voltammetry of an SAE 1010 steel electrode in 0.7 M $NaNO_3$ (solid line) and in 0.10 M calcium benzoate + 0.7 M $NaNO_3$ (dashed line). Scan rate = 0.50 V min^{-1}. Temp. = 20 °C.

0.50 to 1.00 V. In the reverse scan, two cathodic peaks were observed at −0.25 and −0.50 V, denoting the reduction of the iron oxides in aqueous 0.70 M sodium nitrate.

In the same figure is depicted the voltammogram of the steel surface in 0.10 M calcium benzoate + 0.70 M sodium nitrate run at 0.50 V min^{-1}. The electrochemical spectrum shows little activation by iron dissolution. Thus, no anodic peak can be clearly seen, but in the reverse scan a cathodic contribution at ca. −0.6 V is observed. This fact shows the inhibitive action of the benzoate layer on iron dissolution.

Fig. 2a depicts the SEM micrograph of the steel surface after 48 h in contact with sodium nitrate. A compact oxide layer with a smooth morphology, as well as residues of flowerlike and quasi-globular oxides, developed on the steel surface. The structure of the globular formations can be seen with some detail in Fig. 2b. The EDAX analysis revealed that the layer was basically composed of iron oxides. It was not possible to obtain more information with EDAX analysis in this case.

When calcium benzoate was added to the sodium nitrate solution, no signs of the globular oxide appeared after 48 h of exposure. A very smooth and probably thin layer developed on the steel surface, rendering it passive (Fig. 2c). No significant amounts of calcium were detected on the surface by EDAX analysis.

The UV–visible reflectance spectrum of a steel panel (Fig. 3) in contact with the sodium nitrate solution depicted the characteristic absorption bands of iron oxides at 300–400 nm and at ∼ 500 nm [44–46]. On the other hand, the spectrum corresponding to the panel passivated by calcium benzoate showed a band at ∼ 220 nm (Fig. 3), which was reported as a carbonyl group linked to the benzene ring into benzoate compounds [47].

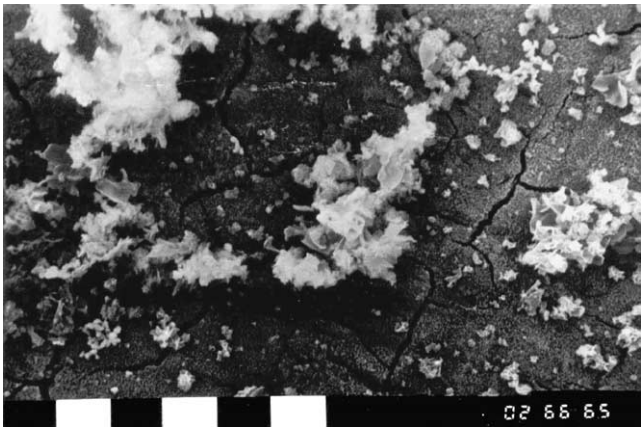

(a)

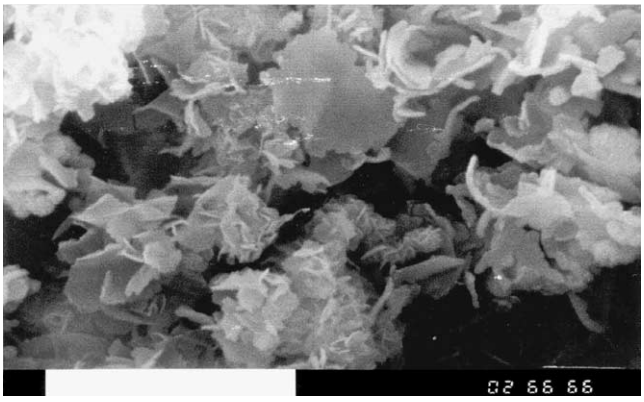

(b)

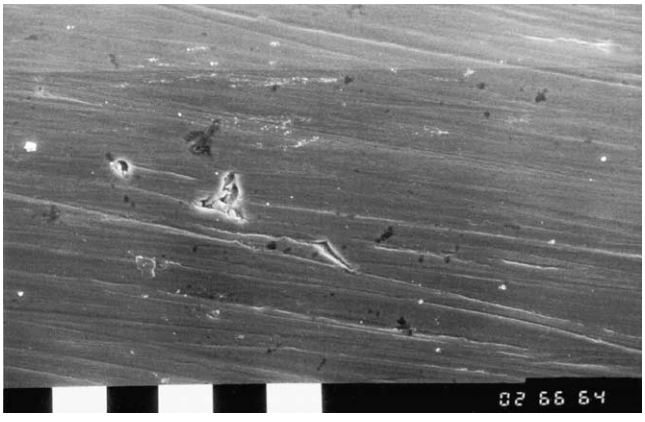

(c)

Fig. 2. SEM micrographs of an SAE 1010 steel surface put in contact with different electrolyte solutions for 48 h: (a) 0.70 M $NaNO_3$ (magnification 1000×), (b) 0.70 M $NaNO_3$ (magnification 5000×), and (c) 0.10 M calcium benzoate + 0.7 M $NaNO_3$ (magnification 1000×).

3.2. Adsorption isotherms for benzoate on SAE 1010 steel in sodium nitrate solutions

3.2.1. Polarization curves of steel in benzoate-containing solutions

A polarization curve of a SAE 1010 steel electrode was run at 0.05 V min^{-1} in oxygenated solutions with different concentrations of calcium benzoate (10^{-5} to 10^{-1} M) + 0.70 M sodium nitrate without forced convection. Fig. 4 shows the Tafel plot (log j vs E) in the presence of calcium benzoate. Table 1 shows the corrosion parameters, j_{corr} and E_{corr}, together with the resulting values of θ, calculated according to Eq. (1) at $t_{ads} = 20$ min.

It can be clearly seen that for increasing benzoate concentrations, the values of j_{corr} decrease monotonically and at $C = 10^{-1}$ M a j_{corr} value results similar to that obtained using $C = 10^{-2}$ M. In the case of E_{corr}, the tendency is to become more positive for increasing C values, clearly denoting the protection of the metal. Concomitantly, θ increased up to 93% for the most concentrated benzoate solution.

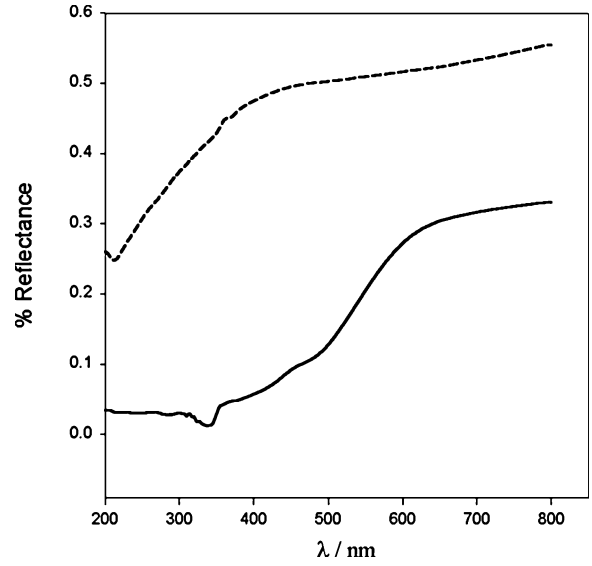

Fig. 3. UV–visible reflectance spectrum of an SAE 1010 steel surface put in contact with different electrolyte solutions for 48 h: 0.70 M $NaNO_3$ (solid line) and 0.10 M calcium benzoate + 0.7 M $NaNO_3$ (dashed line). Temp. = 20 °C.

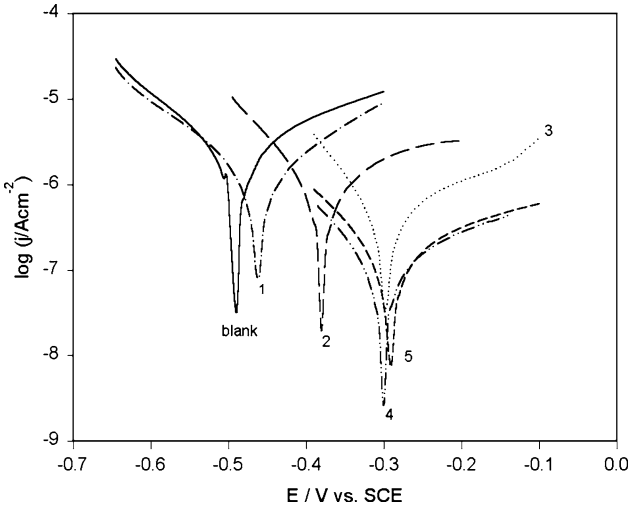

Fig. 4. log j vs E plots of an SAE 1010 steel electrode run at 0.05 V min^{-1} in 0.7 M $NaNO_3$ (solid line as blank) containing different concentrations of calcium benzoate: (1) 10^{-5} M (dashed dotted line); (2) 10^{-4} M (long dashed line); (3) 10^{-3} M (dotted line); (4) 10^{-2} M (dashed doubled dotted line); (5) 10^{-1} M (short dashed line). Temp. = 20 °C. Unstirred solutions.

Table 1
Corrosion parameters and degree of coverage by benzoate on SAE 1010 steel in 0.7 M $NaNO_3$ containing different concentrations of calcium benzoate for 20 min and 20 °C

C (M)	E_{corr} (V vs SCE)	j_{corr} (nA cm^{-2})	θ (%)
0	−0.488	575	–
10^{-5}	−0.463	407	29
10^{-4}	−0.379	229	60
10^{-3}	−0.298	173	70
10^{-2}	−0.303	44	92
10^{-1}	−0.286	39	93

Table 2
Corrosion current densities and surface-coverage values benzoate for a SAE 1010 steel electrode as a function of time (t_{ads})

t_{ads} (min)	j_{corr} (nA cm^{-2})	θ (%)
0	176	–
5	139	21
10	99	43
15	58	67
20	45	89
30	23	90
45	15	91
60	12	93

Note. The coverage (θ) was determined at the open-circuit potential in 0.01 M calcium benzoate + 0.7 M $NaNO_3$ at 20 °C.

On the other hand, Table 2 exhibits another view of the inhibition process. Values of j_{corr} decrease for increasing t_{ads} values under open-circuit conditions using $C = 10^{-2}$ M in 0.70 M sodium nitrate. Moreover, θ matched 90% after 30 min of exposure and reached its maximum value (93%) 30 min later. These data clearly denote the inhibition of steel corrosion under the experimental conditions.

The dependence of θ as a function of t_{ads} can be explained from data of Table 2. For $t_{ads} < 30$ min, θ increases fast with time, whereas for $t_{ads} > 30$ min, the surface coverage reaches a limiting *plateau* value (93%). This behavior can be explained assuming another type of adsorption configuration for the molecule. However, a change in the functional group attachment upon adsorption is not really expected when the potential value of the carboxylate or the aromatic ring toward steel is varied [48]. The interaction of π-bonding states of the aromatic ring with noble metal surfaces has been extensively studied in the case of thin-layer electrochemical interfaces. At potentials larger than that of zero charge of the interface, the aromatic compounds (containing different functional groups) are adsorbed with the phenolic ring parallel to the surface at low concentrations [48]. At these potentials the interaction between the π bonds of the molecule and the d_{z^2} orbital of the metallic atoms is strong enough to stabilize the adsorbed residue without any oxidative disruption [48,49]. On the other hand, when the surface concentration is high enough, reorientation of the aromatic ring takes place normal to the surface [49]. In our case, a similar interaction between benzoate and steel is expected for low surface concentrations of iron oxides. However, we decided to perform semiempirical calculations on simulated cluster surfaces of iron to be sure of our conclusions.

3.2.2. *Evaluation of the adsorption isotherms of benzoate on SAE 1010 steel in sodium nitrate*

The values of θ can also depend on the values of E_{ads}; thus, the influence of the electrode potential on benzoate adsorption was studied at a fixed $t_{ads} = 30$ min, where a plateau is reached.

Values of j_{corr} were calculated at different E_{ads} according to the Experimental section. When $E_{ads} <$ open circuit, the values of j_{corr} are larger than those found at open circuit, and when $E_{ads} \geqslant$ open circuit, almost constant values for j_{corr} are reached. It can be concluded that the optimum value of E_{ads} for benzoate adsorption is the open-circuit potential. At the maximum benzoate coverage, a flat configuration parallel to the surface is expected as explained above. It involves the largest interaction of the two functional groups with the surface, i.e., carboxylate and aromatic ring moieties. This will be calculated by the extended Hückel methodology in another section.

Different types of simple isotherms were assayed to evaluate the best fit of the experimental data. The values of θ used for the fitting procedure correspond to the open-circuit potential at $t_{ads} = 20$ min. The equation obeying those isotherms is

$$\frac{\theta}{(1-\theta)} = KC\exp(-r\theta), \tag{2}$$

where $K = (1/55.5)\exp(-\Delta\bar{G}^0_{ads}/RT)$, $\Delta\bar{G}^0_{ads}$ being the electrochemical standard free energy of adsorption by benzoate on steel, the value 55.5 the molar concentration of the water displaced by benzoate species at the surface, C the bulk concentration of benzoate, T the absolute temperature, and r the lateral interaction parameter for the adsorption process.

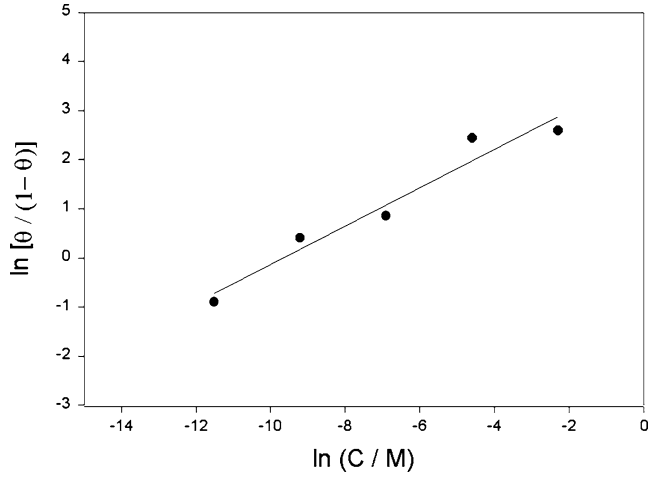

Fig. 5. Adsorption isotherm of calcium benzoate on SAE 1010 steel for a Langmuirian behavior depicted as an $\ln(\theta/1-\theta)$ vs $\ln C$ plot. The open circuit potential is used for 30 min of adsorption in 10^{-2} M calcium benzoate + 0.70 M $NaNO_3$. Temp. = 20 °C. Unstirred solutions.

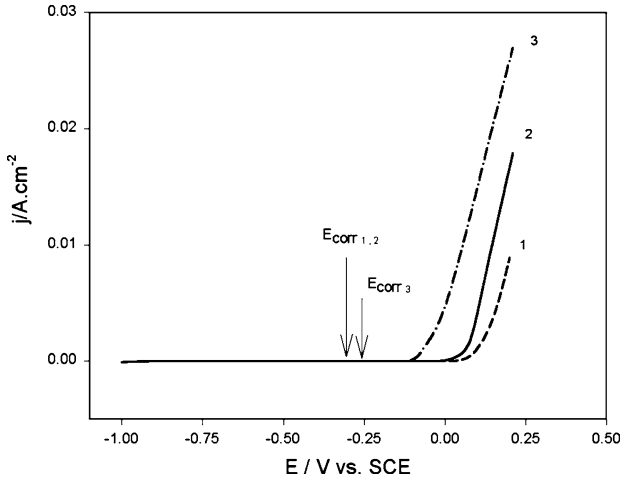

Fig. 6. Linear polarization curves of an SAE 1010 steel electrode run at 0.05 V min^{-1} in different NaCl concentrations: (1) 0.01 M (dashed line); (2) 0.10 M (solid line); (3) 0.40 M (dotted dashed line). The electrode surface has been left for 30 min at the open-circuit potential in 0.10 M calcium benzoate + 0.70 M $NaNO_3$. $E_{corr\,1,2}$ and $E_{corr\,3}$ are the corrosion potentials in 0.01, 0.10, and 0.40 M NaCl, respectively.

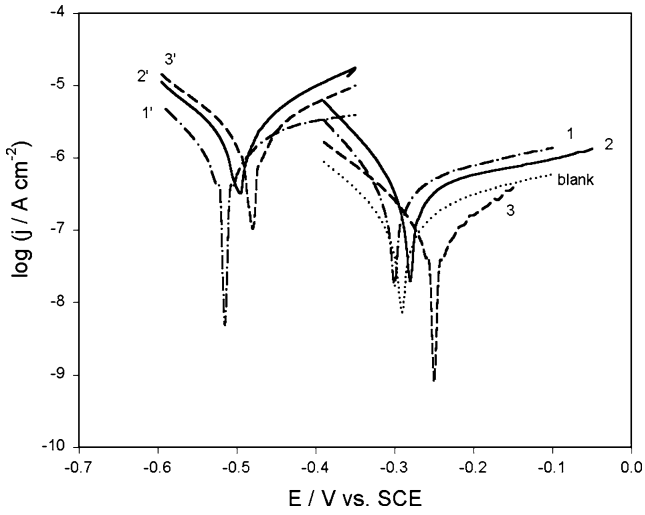

Fig. 7. log j vs E plots of an SAE 1010 steel electrode run at 0.05 V min^{-1} in solutions containing 0.10 M calcium benzoate + 0.70 M $NaNO_3$ + NaCl of (1) 0.01 M (dashed dotted line); (2) 0.10 M (solid line); (3) 0.40 M (dashed line). log j vs E plots of an SAE 1010 steel electrode run at 0.05 V min^{-1} in 0.70 M $NaNO_3$ with different NaCl concentrations: (1′) 0.01 M (dashed dotted line); (2′) 0.10 M (solid line); (3′) 0.40 M (dashed line). The electrode was previously conditioned according to *Routine A*. A blank experiment (dotted line) without growing a benzoate layer is also indicated.

Langmuirian behavior is observed ($r = 0$), since a linear $\ln(\theta/1-\theta)$ vs $\ln C$ plot was obtained (Fig. 5). Then, the equation representing benzoate adsorption on steel is

$$\frac{\theta}{(1-\theta)} = (C/55.5)\exp\left(\frac{-\overline{\Delta G^0_{ads}}}{RT}\right). \tag{3}$$

For Eq. (3) the value of $\Delta\bar{G}^0_{ads} = -32$ kJ mol^{-1} was found, showing a large stabilization of the inhibitor on the steel surface at the open circuit potential.

3.3. *The effect of chloride on steel in nitrate solutions containing benzoate*

Fig. 6 depicts linear polarization curves of an SAE 1010 steel surface in 0.01, 0.10, and 0.40 M sodium chloride solution run from −1.00 to 0.20 V. The interface has been previously left in contact with a 0.10 M benzoate-containing solution at open circuit during 30 min. Calculated E_{corr} values are similar for 0.01 and 0.10 M, −0.30 V. However, when sodium chloride concentration is increased to 0.40 M, $E_{corr} = -0.25$ V. Fig. 6 also exhibits pitting potentials as the abscissa to the sudden increase in the current intensities. The increase in the chloride concentration produces proximity between pitting and corrosion potentials.

3.3.1. *The influence of chloride on steel using* Routine A

Fig. 7 shows the log j vs E plots for the steel surface treated according to *Routine A*. Benzoate was previously adsorbed onto the electrode at the open-circuit potential in two different situations. On one hand, the surface with the benzoate residue was put in contact with different sodium chloride concentrations (0.01, 0.10, and 0.40 M). On the other hand, the electrode was immersed in the same sodium chloride concentrations but in the presence of 0.10 M calcium benzoate. In order to interpret the experimental results with *Routine A*, a blank experiment was also performed without adding calcium benzoate to any testing solutions.

It has been found from the above figure that at sodium chloride concentrations higher than 0.10 M, the inhibitor layer is slightly altered by the pitting agent. In this sense, the values of E_{corr} change from −0.283 to −0.248 V when the chloride concentration is increased from 0.10 to 0.40 M (plots 2 and 3). However, there are small changes when a similar experiment is conducted with calcium benzoate in solution together with sodium chloride. For example, E_{corr} varies from −0.520 to −0.496 V when the chloride concentration is increased from 0.10 to 0.40 M (plots 2′ and 3′). Evidently, when the experiments above are compared (similar chloride concentrations), E_{corr} values are always ca. 0.2 V more positive in the presence of solution benzoate than in the absence. This means that the first layer of the inhibitor (*Routine A*) grown at open circuit for 30 min has a profound effect upon corrosion. Besides, the inhibitor layer can be continuously grown even in the presence of chloride. This can be seen better through j_{corr} values. For example, comparing the experiments run without calcium benzoate in solution at 0.10 M sodium chloride (plot 2′), $j_{corr} = 0.316$ μA cm^{-2}, whereas in the presence of 0.10 M calcium benzoate (plot 2), $j_{corr} = 16.0$ nA cm^{-2}. Also, in a more concentrated sodium chloride solution (0.40 M), j_{corr} values decrease from 100.0 to 1.0 nA cm^{-2}, due to the lower oxygen solubility in the large-ionic-strength electrolyte (higher than 1.2 M). This behavior is not expected but it has been found in other reports [25]. It was explained from the decrease of the mass-

transfer current density with the solubility and diffusion coefficient of soluble oxygen.

3.3.2. The influence of chloride in comparison with results from Routine B

The formation of a steel prepassivated layer previous to the study of the inhibition of benzoate in the presence of sodium chloride (0.40 M) is analyzed in this section. In order to compare corrosion parameters, the same routine was performed in two different cases, first without the inhibitor and second without the pitting agent. Fig. 8 shows the log j vs E plots for *Routine B* in which the surface is subjected to a 0.40 V potential in the two cases pointed above. This figure compares the effect of chloride after passivation in the presence (dotted line, 2) and in the absence (solid line, 1) of the inhibitor. The calculation of corrosion parameters shows a 0.25-V potential shift of E_{corr} to more positive values in the experiment with the inhibitor, and also two orders of magnitude lower j_{corr} values, i.e., from 320 to 0.7 nA cm^{-2}. On the other hand, when no chloride is put in contact with the passivated steel surface after the inhibitor adsorption, the values of E_{corr} are even more stable; that is, -0.282 V, with $j_{corr} = 4.0$ nA cm^{-2}.

In conclusion we can say that the inhibitor remained on the steel surface even after passivation, causing a lower value of j_{corr}. This is an important feature because passivation and inhibition processes in many cases show opposite results.

On the other hand, when performing the same experiment with 0.40 M of chloride after 24 h of resident time, the values $E_{corr} = -0.65$ V and $j_{corr} = 4.4$ μA cm^{-2} are obtained. These corrosion parameters indicate large activities,

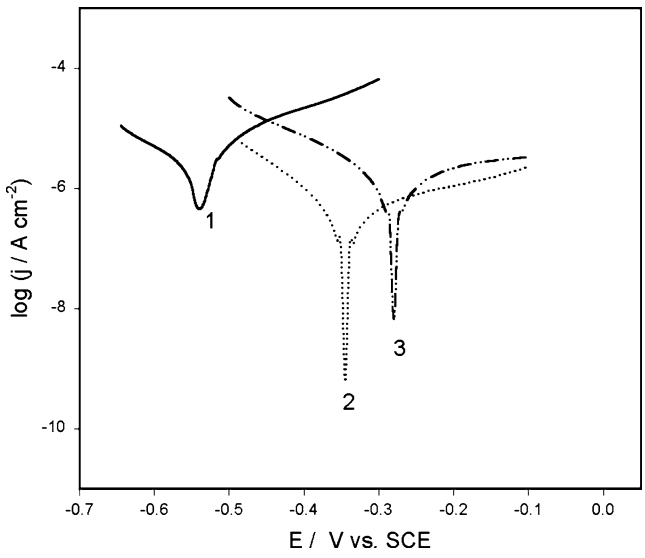

Fig. 8. log j vs E plots of an SAE 1010 steel run at 0.05 V min^{-1} according to *Routine B*. Polarization curves were run under the following conditions: (1) 30 min in 0.70 M $NaNO_3$ followed by 10 min at 0.40 V and 10 min in 0.40 M NaCl (solid line); (2) 30 min in 0.10 M calcium benzoate + 0.70 M $NaNO_3$ followed by 10 min at 0.40 V and 10 min in 0.40 M NaCl (dotted line); (3) 30 min in 0.10 M calcium benzoate + 0.70 M $NaNO_3$ followed by 10 min at 0.40 V (double dotted dashed line).

so the long-term exposure experiments failed in the presence of chloride.

4. Theoretical approach

The confluence of surface science and electrochemistry with molecular orbital theory is bringing a better understanding of the molecular processes at electrode surfaces. One of the simplest methods used in theoretical electrochemistry is the extended Hückel approach [51]. The methodology is the advanced application of the atom superposition and electron delocalization molecular orbital method, where the molecule's energy is calculated as the addition of pairwise repulsive atom superposition and electron delocalization bond formation terms [52].

In this paper, Fe(111) and Fe(100) single crystals are simulated using geometric clusters and the adsorption characteristics of neutral benzoate species on these clusters are predicted by extended Hückel molecular orbital (EHMO) calculations.

Since the EHMO methodology is rather limited, some improvements have been performed before [53], which are explained in detail elsewhere [54]. This improved EHMO procedure was employed to analyze the adsorption of a single benzoate molecule on either an Fe(111) or a Fe(100) cluster surface.

Iron single crystals are simulated by constructing superimposed bilayer Fe_N geometric clusters of $N = 25$ and 32 to model the Fe(111) or the Fe(100) surface, respectively (Fig. 9). Clusters were geometrically built up, keeping constant the Fe–Fe bond length at 0.248 nm [55].

Different adsorption configurations resulting from the occupation of various iron adsorption sites were considered on the surface, that is, the single interaction of the carboxylate group by changing its hybridization to a sp^3 carbon atom (compound A), the aromatic and carboxylate interaction of the planar molecule parallel to the surface (compound B), and linear on-top (onefold), bridge (twofold), and hollow (higher coordination sites) configurations. In all of them the whole aromatic ring is kept as an entire entity. Hollow sites are associated with a fivefold adsorbate coordination on Fe(100) (four iron atoms of the topmost layer and one iron atom from the underlying layer). In the case of Fe(111), either three or four iron atoms may define the hollow coor-

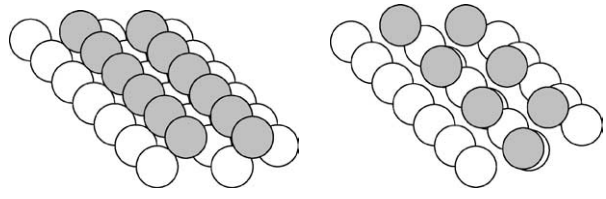

Fig. 9. (a) Fe(100) ($N = 32$) and (b) Fe(111) ($N = 25$) clusters showing the first and second atom layers.

Table 3
Optimized parameters based on an Fe–C bond for EHMO calculations

Atomic orbital	VSIP (eV)	ζ_1	ζ_2	c_1	c_2
Fe3*d*	10.53	5.3750	1.8300	0.6680	0.5510
Fe4*s*	9.36	1.7343			
Fe4*p*	5.82	1.4480			
C2*s*	20.35	1.5670			
C2*p*	10.15	1.5530			
O2*s*	26.46	2.0540			
O2*p*	12.16	2.0670			
H1*s*	12.01	1.2010			

Notes. VSIP ≡ valence state ionization potential. $\zeta_{1,2} \equiv$ orbital exponents of the base generating functions. $C_{1,2} \equiv$ linear coefficients of the double zeta Fe *d*-orbitals.

dination, depending on the local symmetry of the adsorbate, i.e., (3–1) or (3–3) hollow sites, respectively.

Equilibrium valence state ionization potential (VSIP) values were evaluated in the way previously proposed by Anderson and Hoffmann [56]. Benzoate adsorption on iron can involve Fe–C interactions through carbon atoms of the >C=C< (from the aromatic ring) or >C=O moieties and the resulting geometries imply a different polarization of the surface. However, in each case, original VSIP and Slater orbital exponents, assembled in Table 3, define the open-circuit potential of the adsorbed ensembles, all being compared through a parametrization based on the Fe–C bond. The open-circuit potential can be correlated to the experimental open-circuit value of the interface, that is, the electrode potential that results from the interaction between benzoate and iron.

The open-shell configuration of the iron-cluster surface has been considered in the definition of the spin magnetic moment of the $Fe_{N\cdot C_7H_5O_2H}$ adsorbed ensembles [52].

The neutral benzoate binding energies (BE) were calculated according to the equation:

$$\mathrm{BE} = E_{\mathrm{T},\mathrm{Fe}_{N\cdot C_7H_5O_2H}} - E_{\mathrm{T},\mathrm{Fe}_N} - E_{C_7H_5O_2H}, \qquad (4)$$

where $E_{\mathrm{T},\mathrm{Fe}_{N\cdot C_7H_5O_2H}}$ and $E_{\mathrm{T},\mathrm{Fe}_N}$ are the total energies of the $[\mathrm{Fe}_{N\cdot C_7H_5O_2H}]$ and $[\mathrm{Fe}_N]$ clusters, and $E_{C_7H_5O_2H}$ is obtained from the energy of the free organic molecule.

The geometries of the adsorbed ensembles were optimized to minimum energy. This implies the simultaneous modification of C–C, C–O, C=O, O–H, and Fe–C bond lengths, r_{CC}, r_{CO}, $r_{C=O}$, r_{OH} and r_{FeC}, respectively; and Fe–C=C, O–C–C, and C–C(O)–C planar angles, $\alpha_{Fe-C=C}$, α_{O-C-C}, and $\alpha_{C-C(O)-C}$, respectively. No dihedral angles were optimized, to avoid the distortion and oxidative disruption of the molecule. For the analysis of the optimal geometry of each ensemble, r_{CC}, r_{CO}, $r_{C=O}$, and r_{OH} were varied in 0.001-nm increments until minimum energy was attained. The Fe–C bond length was first kept at 0.180 nm and a distortion of the benzoate molecule was imposed by simultaneous linear variation of all geometric coordinates, but not in the case of the aromatic ring. For each fixed r_{FeC} value, the remaining internal coordinates were fully optimized again.

5. Results of the calculations

5.1. The interaction of a single benzoate molecule with an Fe(111) or an Fe(100) cluster surface

EHMO calculations conducted for the free benzoate molecule lead to the equilibrium bond lengths $r_{CC} = 0.142$ nm, $r_{C=C} = 0.126$ nm, $r_{C=O} = 0.117$ nm, $r_{CO} = 0.126$ nm, $r_{OH} = 0.104$ nm, and $r_{CH} = 0.108$ nm. The planar angles are nearly those expected for a conjugated molecule; that is, $\alpha_{H-C=C} = 120°$ and $\alpha_{C-C(O)-O} = 117°$. The representation of the planar molecule with its associated geometric characteristics is shown in Fig. 10.

From the analysis of the charge populations on the different atoms of the metal and the adsorbate, the following conclusions derive. The interaction of benzoate with an iron cluster involves the donation and back-donation of electronic charge from the >C=C< and >C=O functional groups of the molecule to the metal, and vice versa. The donation takes place via electron transfer from the π orbitals of the adsorbate to the unoccupied metal *d* orbitals, whereas the back-donation populates the π^* orbitals of the adsorbate with electrons from the occupied metal orbitals. Both interactions and electron transfers are attractive processes and the contribution of the repulsion is only the result of the interaction between occupied orbitals of the adsorbate and the metal.

On the other hand, the adsorption of the flat molecule parallel to the surface by the simultaneous interaction of >C=C<, >C–C<, and >C=O groups involves at least five surface atoms (Fig. 11). This type of adsorbate is interesting

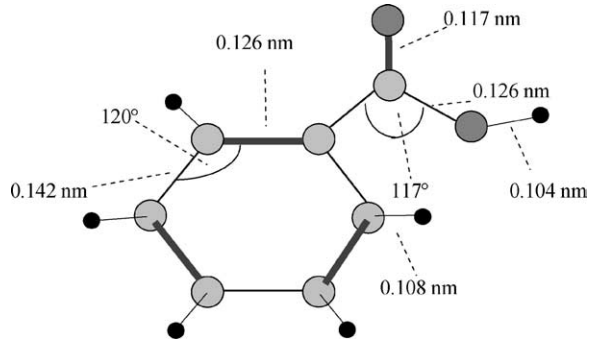

Fig. 10. Geometric characteristics of the free benzoate molecule. Dark gray balls represent C atoms and middle-dark gray balls O atoms.

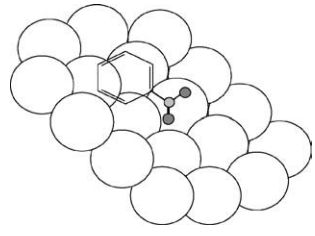

Fig. 11. Benzoate adsorption via the carboxylate group on an Fe(111) cluster. White balls are the Fe atoms, the middle-dark gray ball is the C atom, and dark gray balls are O atoms. H atoms are omitted for simplicity. Wide bars represents double bonds and narrow bars represent single bonds.

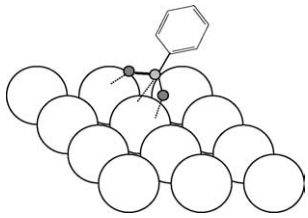

Fig. 12. Flat configuration for benzoate species on an Fe(111) cluster. White balls are the Fe atoms, the middle-dark gray ball is the C atom, and the dark gray balls are O atoms. H atoms are omitted for simplicity. Wide bars represents double bonds and narrow bars single bonds.

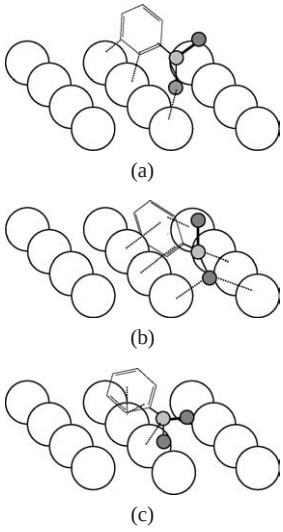

Fig. 13. Adsorption modes of benzoate species on Fe clusters: di-σ, μ-bridging, π-modes. White balls are the first layer of Fe atoms, the middle-dark gray ball is the C atom, and the dark gray balls are O atoms. H atoms are not drawn.

for the explanation of the high surface coverage seen for this molecule on our experiments.

The adsorption of the molecule through the carboxylate group only leads to the opening of the double carbonyl bond and to the formation of a sp^3 carbon atom. The binding of the new >C<$^{O-}$ group to the surface involves two Fe atoms, yielding a different structure, which is depicted in Fig. 12.

Three modes of coordination have also been tested for benzoate adsorption through only the interaction of the >C=C< moiety with the Fe(111) or the Fe(100) cluster surface. The di-σ configuration involves the interaction of three iron atoms by σ bonds with the aromatic ring and one oxygen atom (Fig. 13a). The π configuration (Fig. 13c) involves only the interaction of the π bond of the aromatic moiety with one iron atom and one oxygen atom with another iron. Because of the sp^2 character of the molecule, another type of configuration is also possible, a μ-bridging configuration, where each carbon atom can bind to two iron atoms in a hollow position through π and σ bonds (Fig. 13b). The consequence of the donation and back-donation processes is the weakening of the C–C bond strength (the bond between the aromatic and carboxylate moieties), increasing the corresponding bond length, and the simultaneous formation of Fe–C=O bonds.

The main difference between π, di-σ, and μ-bridging configurations arises from the existence of C=C and C–C bond lengths in the aromatic ring that can interact through σ and π orbitals with four iron atoms together with the carboxylate moiety with two more metal atoms. However, in the three configurations the carbonyl species has a lower interaction energy and only screens the adjacent iron atom.

The geometric characteristics and BE values for benzoate, calculated from Eq. (4), are assembled and compared in Table 4 for both Fe(111) and Fe(100) clusters. For the first three configuration modes, larger BE values on Fe(100) cluster surfaces are observed; however, greater stability is achieved for the π configuration on both cluster surfaces. Thus, the >C=C< bond length in di-σ and μ-bridging configurations nearly corresponds to the bond length of a saturated molecule, whereas in the π configuration it is very near to that for an undistorted ethylene molecule. On the other hand, the >C=O bond length is much greater than expected on the two cluster surfaces.

To get deeper insight into the adsorption characteristics of benzoate adsorbates, the charge populations of each atom was examined. If we compare the charges involved on the carbon, oxygen, and hydrogen atoms before and after benzoate adsorption, it can be concluded that the overall charge transfer for the adsorption on both iron cluster surfaces is originated from a back-donation process. In this respect, the total electrons of the back donation are located on carbon atoms of the aromatic moiety. For example, the electrons donated from the π orbitals of the μ-bridging configuration to

Table 4
Neutral benzoate binding energies, BE (eV), and optimized distances and angles, r_{AB} (nm) and $\alpha_{A–B–C}$ (°), on Fe(111) and Fe(100) at the open circuit potential

	BE	$r_{Fe–C\phi}$	$r_{Fe–O}$	$r_{\phi C–C(O)}$	$r_{C=O}$	$r_{O–H}$	$\alpha_{Fe–C–C}$	$\alpha_{C–C(O)–O}$
				Fe(111)				
di-σ	−2.0563	0.171	0.167	0.148	0.118	0.105	120	115
π	−2.3534	0.180	0.178	0.141	0.127	0.104	109	122
μ-bridging	−2.2348	0.184	0.189	0.163	0.122	0.109	89	109
				Fe(100)				
di-σ	−2.2121	0.167	0.162	0.145	0.117	0.104	121	114
π	−2.5457	0.178	0.175	0.140	0.129	0.103	110	120
μ-bridging	−2.3865	0.180	0.183	0.161	0.121	0.108	90	110

Table 5
Benzoate binding energies, BE (eV), and optimized distances and angles, r_{AB} (nm) and $\alpha_{A–B–C}$ (°), on Fe(111) and Fe(100) at equilibrium potentials

	BE	$r_{Fe–C\phi}$	$r_{Fe–O}$	$r_{\phi C–C(O)}$	$r_{C=O}$	$r_{O–H}$	$\alpha_{Fe–C–C}$	$\alpha_{C–C(O)–O}$
				Fe(111)				
Flat config.	−3.6876	0.156	0.152	0.150	0.142	0.106	92	120
Carboxylate config.	−2.0024	0.188	0.148	0.154	0.126	0.102	–	135
				Fe(100)				
Flat config.	−3.7332	0.154	0.150	0.151	0.145	0.105	91	120
Carboxylate config.	−2.0211	0.186	0.144	0.156	0.127	0.103	–	137

the iron atoms is half of the number back-donated to the π^* from the metal. In the case of the di-σ species, the contribution of the π^* back-donation is only ca. 30% lower than the electron donation to the π orbitals, but both processes are stronger than those found on the μ-bridging configuration. Molecular orbital analysis shows that p_x and p_z orbitals (in the plane of the molecule) of the benzoate molecule are involved by bonding interaction with d_{xz} and $d_{x^2-y^2}$ atomic platinum orbitals. The larger Fe–C bond length in the μ-bridging configuration produces a lower net charge on the involved iron atoms than that produced on the other configurations. This effect is more pronounced on Fe(111) than on Fe(100) clusters, since a larger BE is developed on the latter.

The flat configuration is formed by the single interaction of the carboxylate group of neutral benzoate with two adjacent iron atoms and the aromatic ring with two metal atoms. This strong interaction increases the C=O bond length to almost larger than that of a single C–O bond and strengthens the Fe–C and Fe–O bonds. In this case, more stable adsorbates are formed on Fe(100) surfaces due to the smaller Fe–O and Fe–C bond lengths (see Table 5).

On the other hand, the interaction of the carboxylate moiety lying normal to the surface with iron atoms, that is, the interaction of >C=O with two iron atoms, yields another adsorbate depicted in Fig. 12. This adsorbate screens fewer iron surface atoms than the flat configuration, resulting in the lowest BE (see Table 5). However, the difference in the BE values between Fe(111) and Fe(100) is smaller than for those adsorbates involving the two combined interactions of the aromatic and carboxylate moieties. This is the consequence of the lower coordination number of this type of adsorbate.

6. Conclusions

(1) The voltammetric profile of steel in calcium benzoate solutions showed little activation by iron dissolution, thus pointing out the inhibitive action of calcium benzoate.
(2) The maximum surface coverage degree by calcium benzoate was found to be 0.93 after 30 min. The adsorption of calcium benzoate on SAE 1010 steel electrode was found to be of a Langmuirian type. The calculated value of $\Delta\bar{G}^0_{ads}$ was $-32\ kJ\ mol^{-1}$, showing a large stabilization of the benzoate on steel.
(3) In order to achieve better results, the suggested concentration of the inhibitor on steel lies between 10^{-2} and 10^{-1} M. The best performance of the inhibitor was found to occur at the open-circuit potential. The increase of the electrode potential produced a fast increase in the corrosion current density.
(4) The presence of chloride after 24 h of exposure exhibited a restricted effect on the protective properties caused by calcium benzoate either on the surface or in solution.
(5) Extended Hückel molecular-orbital calculations of a benzoate molecule on simulated Fe(100) and Fe(111) single crystals show that the most probable benzoate adsorbate is that of a flat molecule, where the carboxylate moiety interacts with two iron atoms and the aromatic ring with two more surface atoms.
(6) The binding energies calculated from the extended Hückel methodology on Fe(100) are larger than those found on Fe(111). The overall charge transfer during adsorption originates from a back-donation process. The total electrons of the back donation are located mostly on carbon atoms of the aromatic moiety.

Acknowledgments

The authors thank the CIC (Comisión de Investigaciones Científicas de la Provincia de Buenos Aires, Argentina), the UNLP (Universidad Nacional de La Plata), and the Universidad de la República of Uruguay for their financial support. G.B. also thanks RELACQ for a fellowship.

References

[1] H.H. Uhlig (Ed.), The Corrosion Handbook, Wiley, New York, 1948, pp. 125–207.
[2] L.L. Shreir (Ed.), Corrosion, vol. 2: Corrosion Control, Newnes–Butterworths, 1976, chapter 18.
[3] W. Flick, Corrosion Inhibition. An Industrial Guide, second ed., Noyes, 1993.
[4] H. Kaesche, in: Metallic Corrosion. Principles of Physical Chemistry and Current Problems, NACE, Houston, TX, 1985, chapter 7.
[5] I.L. Rozenfeld (Ed.), Corrosion Inhibitors, McGraw–Hill, New York, 1981.
[6] G. Trabanelli, V. Carasetti, in: M.G. Fontana, R.W. Staehle (Eds.), Advances in Corrosion Science and Technology, vol. 1, Plenum, New York, 1970, p. 147.

[7] S.L. Granese, B.M. Rosales, C. Oviedo, J.O. Zerbino, Corros. Sci. 33 (1992) 1439.
[8] F. Bentiss, M. Lagrenee, M. Traisnel, J.C. Hornez, Corrosion (NACE) 55 (1999) 968.
[9] R. Manickvasagam, K. Jeyakarthic, M. Paramasivam, S. Venkatakrishna Iyer, Anti-Corros. Methods Mater. 49 (2002) 19.
[10] M.N. Desai, M.B. Desai, Corros. Sci. 24 (1984) 649.
[11] M. Abdallah, A.A. El-Sarawy, A.Z. El-Sonbati, Corros. Prev. Control 48 (2001) 97.
[12] T. Szauer, Z. Klenowicz, Z. Szlarska-Smialowska, Corrosion (NACE) 36 (1980) 400.
[13] M. Metikos, R. Babic, Z. Grubac, S. Brinic, J. Appl. Electrochem. 26 (1996) 443.
[14] B. Donelly, T.C. Downie, R. Grehowiak, D. Short, Corros. Sci. 14 (1974) 597.
[15] J.C. Lin, S.L. Chang, S.L. Lee, J. Appl. Electrochem. 29 (1999) 911.
[16] A. Singh, R.S. Chaudhary, Brit. Corros. J. 31 (1996) 300.
[17] R. Agrawal, T.K.G. Namboodhiri, J. Appl. Electrochem. 27 (1997) 1265.
[18] M.A. Quraishi, J. Rawat, M. Ajmal, Corrosion (NACE) 54 (1998) 996.
[19] M.G. Fontana, N.D. Greene, Corrosion Engineering, McGraw–Hill, New York, 1978, chapter 6, pp. 200–202.
[20] M. Amalhay, I. Ignatiadis, Electrochemical Methods in Corrosion Research, vols. I and II, in: P.L. Bonora, F. Deflorian (Eds.), Materials Science Forum, vols. 289–292, 1998, pp. 169–180.
[21] M.W. Kendig, A.T. Allen, S.C. Jeanjaquet, F. Mansfeld, in: R. Baboian (Ed.), Electrochemical Techniques for Corrosion Engineering, NACE, Houston, TX, 1986, pp. 151–160.
[22] G.R. Cameron, A.S. Chiu, in: R. Baboian (Ed.), Electrochemical Techniques for Corrosion Engineering, NACE, Houston, TX, 1986, pp. 183–189.
[23] J.O'M. Bockris, M.A. Habib, J.L. Carbajal, J. Electroanal. Chem. 131 (1993) 81.
[24] B.R. Sharifker, M.A. Habib, J.L. Carbajal, J.O'M. Bockris, Surf. Sci. 173 (1986) 97.
[25] D. Eurof Davies, Q.J.M. Slaiman, Corros. Sci. 13 (1973) 891.
[26] D. Eurof Davies, Q.J.M. Slaiman, Corros. Sci. 11 (1971) 671.
[27] P. Agarwal, D. Landolt, Corros. Sci. 40 (1998) 673.
[28] C.-O.A. Olson, P. Agarwal, M. Frey, D. Landolt, Corros. Sci. 42 (2000) 1197.
[29] O. Lahodny-Šarc, F. Kapor, Mater. Sci. Forum 289–292 (1998) 1205.
[30] D.S. Azambuja, L.R. Holzle, I.L. Müller, C.M. Piatnicki, Corros. Sci. 41 (1999) 2083.
[31] P.N.S. Yadav, A.K. Singh, R. Wadhwani, Corrosion 55 (1999) 937.
[32] V.S. Muralidharan, R. Sethuraman, S. Krishnamoorthy, Bull. Electrochem. 4 (1988) 705.
[33] A.K. Mohamed, S.A. Abd El-Maksoud, A.S. Fonda, Port. Electrochim. Acta 15 (1997) 27.
[34] I.A. Raspini, Corrosion 49 (1999) 821.
[35] B. Sanyal, Prog. Org. Coat. 9 (1981) 166.
[36] S.A. Hodges, W.M. Uphues, M.T. Tran, Surf. Coat. Int. 80 (1997) 178.
[37] D. Darling, R. Rakshpal, Mater. Perform. 37 (12) (1998) 42.
[38] E. Śmieszek, M. Zubielewicz, Farbe und Lack 102 (1996) 81.
[39] A. Braig, Prog. Org. Coat. 34 (1998) 13.
[40] H. Leidheiser Jr., J. Coat. Technol. 53 (678) (1981) 29.
[41] Z. Szklarska-Smialowska, J. Mankowsky, Brit. Corros. J. 4 (1969) 271.
[42] S. Gee, Surf. Coat. Int. 80 (1997) 316.
[43] J.O. Zerbino, J.R. Vilche, J. Appl. Electrochem. 11 (1981) 703.
[44] C.A. Borrás, R. Romagnoli, R.O. Lezna, Electrochim. Acta 45 (2000) 1717.
[45] G. Kortüm, Reflectance Spectroscopy, Springer-Verlag, New York, 1969.
[46] G. Larramona, C. Gutiérrez, J. Electrochem. Soc. 136 (1981) 2171.
[47] J.W. Cooper, Spectroscopic Techniques for Organic Chemists, 110, Wiley–Interscience, New York, 1980, pp. 67–69.
[48] M.P. Soriaga, P.H. Wilson, A.T. Hubbard, J. Electroanal. Chem. 142 (1982) 317.
[49] V. Chia, J.H. White, M.P. Soriaga, A.T. Hubbard, J. Electroanal. Chem. 217 (1987) 121.
[50] W.W. Frenier, F.B. Growcock, V.R. Lopp, Corrosion (NACE) 44 (9) (1988) 590.
[51] R. Hoffman, J. Phys. Chem. 39 (1963) 1797.
[52] G. Calzaferri, L. Forss, Y. Kamber, J. Phys. Chem. 93 (1989) 5366.
[53] T.A. Gurner, Methods in Molecular Orbital Theory, Prentice–Hall, Englewood Cliffs, NJ, 1974.
[54] C.F. Zinola, G.L. Estiú, E.A. Castro, A.J. Arvia, J. Phys. Chem. 98 (1994) 1766.
[55] D.R. Lide (Ed.), Handbook of Chemistry and Physics, CRC Press, Boca Raton, FL, 1990–1991.
[56] A.B. Anderson, R. Hoffmann, J. Chem. Phys. 60 (1974) 4271.